Absolute Binding Energies of Alkali-Metal Cation Complexes with Benzene Determined by Threshold Collision-Induced Dissociation Experiments and ab Initio Theory

Jay C. Amicangelo and P. B Armentrout*

Department of Chemistry, University of Utah, Salt Lake City, Utah 84112

Received: July 25, 2000; In Final Form: September 28, 2000

The sequential bond dissociation energies (BDEs) of the mono- and bis-benzene complexes with alkali metal cations (Li^+, Na^+, K^+, Rb^+, and Cs^+) are determined experimentally by collision-induced dissociation (CID) with Xe in a guided ion beam mass spectrometer and theoretically by ab initio calculations. The kinetic energy dependence of the CID cross sections are analyzed to yield 0 and 298 K bond energies for $(C_6H_6)_{x-1}M^+-C_6H_6$ ($x = 1-2$) after accounting for the effects of the internal energies of the reactant ions, the multiple collisions of the ions with xenon, and the dissociation lifetimes of the ionic complexes. Ab initio binding energies are calculated at the MP2(full)/6-311+G(2d,2p)//MP2(full)/6-31G* level and corrected for zero-point energies (ZPE) and basis set superposition errors (BSSE). The theoretical BDEs are in reasonably good agreement with the experimentally determined 0 K bond energies when full electron correlation is included (for Li^+, Na^+, and K^+) but differ appreciably when effective core potentials (ECPs) are used for the K^+, Rb^+, and Cs^+ metal ions. The trends in $M^+(C_6H_6)_x$ binding energies are explained in terms of varying magnitudes of electrostatic interactions and ligand−ligand repulsions in the complexes. Agreement between our BDEs and the few previous experimental $M^+(C_6H_6)_x$ BDEs is found to be good in most cases. Comparisons are also made to previous theoretical $M^+(C_6H_6)_x$ BDEs in the literature and to the experimental BDEs of alkali-metal ion−water and alkali-metal ion−dimethyl ether complexes.

Introduction

Molecular recognition has now become an extensively researched field of chemistry.[1,2] An important practical application of molecular recognition is in the design and implementation of new chemical separation strategies for the removal of radioactive and heavy-metal ions from waste water streams.[3] This generally involves the development of new ligands or host systems that can effectively and efficiently bind the metal ions of interest, thereby removing them from the aqueous environment. This strategy implies that the binding strength of the ligand or host must be greater than or comparable to the aqueous solvation energy of the metal ion.

Two classes of compounds which show potential in this regard are calixarenes[4−8] and cyclophanes.[4,9] These compounds are "cage-like" structures in which the "walls" are composed of aromatic rings. It has been demonstrated that compounds of this type can strongly bind cations, both organic and metallic (including alkali metals), in both aqueous and organic environments and that the aromatic portions of these structures account for a large portion of the binding.[4,8] This type of noncovalent cation−π interaction has also been implicated as a substantial driving force in several biological systems involving the binding of cations.[4,10,11]

To aid in the development of these types of hosts, fundamental insight into the nature and strength of cation−π interactions is necessary. This can be accomplished with gas-phase studies of ion−molecule complexes in which the neutral ligand binds through its π electrons. Benzene is the simplest of the aromatic ligands that could mimic the binding properties of π ligands such as calixarenes and cyclophanes. Several earlier gas-phase experimental studies have shown that the binding of lithium,[12,13] sodium,[14,15] and potassium[16] ions with benzene is indeed strong and comparable to the bond strengths of these metal ions with more typical coordinating functional groups, such as amines, ethers, alcohols, and water. Complementary to the gas-phase experimental studies are high-level theoretical calculations, which have been performed for several of the alkali-metal ion complexes with benzene at various levels of theory.[4]

The present work was undertaken in order to obtain a more comprehensive determination of the intrinsic bond strengths of the alkali-metal ion (Li^+ through Cs^+) complexes with one and two benzene ligands. This is because there are no previous determinations of the bond energies for monobenzene complexes with Rb^+ or Cs^+, and the only determination for bis-benzene complexes with the alkali-metal ions is for K^+.[16] Here, the bond dissociation energies (BDEs) are determined experimentally using threshold collision-induced dissociation and theoretically using ab initio calculations.

Experimental Methods

General. The guided ion beam instrument on which these experiments were performed has been described in detail previously,[17,18] except for a modification of the octopole ion guide, the experimental details of which will be described in a future publication.[19] Ions are created in a dc-discharge/flow tube ion source, as described below. After being extracted from the source, the ions are accelerated and passed through a magnetic sector for mass analysis. The mass-selected ions are then decelerated to the desired kinetic energy and focused into an octopole ion beam guide. This device uses radio-frequency electric fields to trap the ions in the radial direction and ensure complete collection of reactant and product ions.[20] The current

10.1021/jp002652f CCC: $19.00
Published on Web 11/08/2000

TABLE 1: Parameters Used in Eq 1 to Fit $M^+(C_6H_6)_x$ CID Cross Sections, Threshold Dissociation Energies at 0 K, and Entropies of Activation at 1000 K[a]

complex	σ_0[b]	n[b]	E_0[c](eV)	E_0 (PSL) (eV)	$\Delta S^{\ddagger}$ (PSL) (J mol^{-1} K^{-1})
$Li^+(C_6H_6)$	3.0 (0.7)	1.5 (0.2)	1.69 (0.14)	1.67 (0.14)	47 (2)
$Na^+(C_6H_6)$	12.5 (0.4)	1.3 (0.1)	0.96 (0.06)	0.96 (0.06)	43 (2)
$Na^+(C_6H_6)$[d]	14.3 (1.3)	1.2 (0.1)	0.92 (0.05)	0.92 (0.05)	50 (3)
$K^+(C_6H_6)$	30.6 (0.6)	1.0 (0.1)	0.76 (0.04)	0.76 (0.04)	33 (2)
$Rb^+(C_6H_6)$	17.3 (0.7)	1.0 (0.1)	0.71 (0.04)	0.71 (0.04)	24 (2)
$Cs^+(C_6H_6)$	23.1 (0.3)	1.0 (0.1)	0.67 (0.05)	0.67 (0.05)	20 (2)
$Li^+(C_6H_6)_2$	128 (10)	1.0 (0.1)	1.11 (0.07)	1.08 (0.07)	58 (4)
$Na^+(C_6H_6)_2$	230 (22)	1.0 (0.1)	0.84 (0.06)	0.83 (0.06)	64 (8)
$K^+(C_6H_6)_2$	146 (7)	0.70 (0.09)	0.71 (0.07)	0.70 (0.07)	68 (8)
$Rb^+(C_6H_6)_2$	92 (2)	0.61 (0.06)	0.66 (0.08)	0.65 (0.08)	70 (8)
$Cs^+(C_6H_6)_2$	105 (4)	0.63 (0.05)	0.62 (0.08)	0.61 (0.08)	71 (8)

[a] Uncertainties in parentheses. [b] Average values for the loose PSL transition state. [c] No RRKM analysis. [d] Values taken from previous CID work, ref 15.

arrangement consists of two consecutive octopole ion guides rather than the single octopole present in the previous configuration. The lengths of the first and second octopoles are 22.9 and 63.5 cm, respectively, and the distance between them is 1.0 mm. The RF voltage is the same for the two octopoles, but the DC voltage on the second octopole is slightly more negative (by 0.3 V) for the current experiments. The first octopole passes through a gas cell of effective length 8.26 cm that contains the neutral collision partner, Xe, at a fairly low pressure (0.05−0.2 mTorr). The unreacted parent and product ions drift to the end of the second octopole, from which they are extracted, passed through a quadrupole mass filter for mass analysis, and detected with a secondary electron scintillation ion detector using standard pulse-counting techniques. Raw ion intensities are converted to cross sections, as described previously.[17] Absolute cross section magnitudes are estimated to be accurate to ±20% for all ions other than Li^+, while relative cross sections are accurate to ±5%. The cross sections for the formation of Li^+ show more deviations in magnitude than is typical for this apparatus, and therefore, the accuracy of the absolute magnitudes of Li^+ formation are likely to be ±50%. This is because the radio frequency used for the octopole does not trap light masses with high efficiency, resulting in increased product losses. It has been verified that the energy profiles (and thus the threshold analyses) of the Li^+ product cross sections are not affected by these variations in magnitude.[21,22]

Laboratory (lab) energies are converted to center-of-mass (CM) energies using the conversion $E_{CM} = E_{lab}M/(M + m)$, where M and m are the neutral and ion masses, respectively. All energies cited below are in the CM frame unless otherwise noted. The absolute energy scale and corresponding full width at half-maximum (fwhm) of the ion beam kinetic energy distribution are determined using the octopole as a retarding energy analyzer, as described previously.[17] Because the reaction zone and the energy analysis region are physically the same, ambiguities in the energy analysis resulting from contact potentials, space charge effects, and focusing aberrations are minimized.[17] The energy distributions are nearly Gaussian and have typical fwhms of 0.20−0.35 eV (lab).

It has previously been shown[23−25] that the shape of collision-induced dissociation (CID) cross sections of ionic complexes is often affected by multiple collisions with the neutral reactant gas, even when the neutral gas pressure is fairly low. Because the presence and magnitude of these pressure effects is difficult to predict, we have performed pressure-dependent studies of all cross sections examined here. In the present systems, we found slight to marked dependence on the xenon pressure in the collision cell. Data free from pressure effects are obtained by extrapolating to zero reactant pressure, as described previously.[24] In the case of the $M^+(C_6H_6)$ systems, three xenon pressures were used, 0.20, 0.10, and 0.05 mTorr. For the $M^+(C_6H_6)_2$ ions, only the latter two pressures were used because at the highest pressure, the primary product intensity was greater than 15% of the reactant ion beam intensity. At such high product intensities, tertiary collisions can become important, preventing a true linear extrapolation to zero pressure. All cross sections shown below and all threshold analyses reported here are for data that have been extrapolated to zero pressure and therefore represent rigorously single-collision conditions.

Ion Source. The alkali-metal benzene ions are formed in a 1 m long flow tube[18,24] operating at a pressure of 0.6−0.8 Torr with helium flow rates of 6500−7500 sccm. Alkali metal ions are generated in a continuous dc discharge by argon ion sputtering of a tantalum cathode with a cavity containing the alkali metal for Li, Na, and K or the alkali metal chloride salt for Rb and Cs. Typical operating conditions of the discharge source are 1.8−2.5 kV and 12−22 mA in a flow of roughly 10% argon in helium. Benzene vapor is introduced into the flow approximately 50 cm downstream from the dc discharge, and the $M^+(C_6H_6)_x$ complexes are formed by associative reactions of the alkali metal cations with benzene, which are stabilized by collisions with the surrounding bath gas. The flow conditions used in this ion source provide approximately $0.5-1 \times 10^5$ collisions with the He buffer gas, so the ions are believed to be thermalized both vibrationally and rotationally to 300 K. In our analysis of the data, we assume that the ions are in their ground electronic states and that their internal energy is well characterized by a Maxwell−Boltzmann distribution of ro-vibrational states at 300 K. Previous work from this laboratory has shown that these assumptions are generally valid.[23,25−28]

Thermochemical Analysis. The threshold regions of the collision-induced dissociation cross sections are modeled using

$$\sigma(E) = \sigma_0 \sum_i g_i (E + E_i - E_0)^n / E \qquad (1)$$

where σ_0 is an energy-independent scaling factor, E is the relative translational energy of the reactant ion and neutral, E_0 is the CID threshold at 0 K, and the exponent n is an adjustable parameter. The summation is over the ro-vibrational states of the reactant ion, i, where E_i and g_i are the energy and the population ($\Sigma g_i = 1$) of each state, respectively. The populations of ro-vibrational excited levels are not negligible at 300 K as a result of the many low-frequency modes present in these alkali-metal benzene ions. The relative reactivities of all ro-vibrational states, as reflected by the parameters σ_0 and n, are assumed to be equivalent. Vibrational frequencies (Table 1S) and rotational

TABLE 2: Geometrical Parameters of MP2(full)/6-31G* and MP2(full)/6-311+G* Optimized Structures of the $M^+(C_6H_6)_x$ Complexes

	M−C (Å)		M-Centroid (Å)[a]		C−C (Å)		C−H OOP Angle (deg)[b]	
complex	6-31G*	6-311+G*	6-31G*	6-311+G*	6-31G*	6-311+G*	6-31G*	6-311+G*
C_6H_6					1.395	1.399	0.00	0.00
$Li^+(C_6H_6)$	2.371	2.318	1.910	1.842	1.405	1.407	0.95	0.49
$Na^+(C_6H_6)$	2.757	2.775	2.373	2.394	1.403	1.405	2.19	1.90
$K^+(C_6H_6)$	3.167	3.141	2.841	2.810	1.400	1.403	2.27	2.33
$K^+(C_6H_6)^c$	3.194	3.218	2.870	2.896	1.401	1.403	2.21	2.60
$Rb^+(C_6H_6)^c$	3.431	3.462	3.132	3.165	1.401	1.402	2.41	2.57
$Cs^+(C_6H_6)^c$	3.671	3.693	3.394	3.417	1.400	1.402	2.32	2.49
$Li^+(C_6H_6)_2$	2.402	2.376	1.950	1.917	1.402	1.405	0.92	0.32
$Na^+(C_6H_6)_2$	2.744	2.799	2.359	2.421	1.402	1.405	1.99	1.44
$K^+(C_6H_6)_2$	3.177	3.160	2.852	2.832	1.400	1.403	2.03	2.19
$K^+(C_6H_6)_2^c$	3.202	3.237	2.879	2.917	1.401	1.402	1.97	2.45
$Rb^+(C_6H_6)_2^c$	3.446	3.406	3.149	3.105	1.401	1.402	2.03	2.02
$Cs^+(C_6H_6)_2^c$	3.692	3.670	3.416	3.392	1.400	1.402	2.01	2.15

[a] The metal ring−centroid distance is defined as the distance from the metal atom to the central point within the benzene ring that is in the plane of the carbon atoms. [b] Out-of-plane angle. [c] The Hay−Wadt ECP/valence basis set was used for the metal atom, as described in the text, and the 6-31G* or 6-311+G* basis set for C and H.

constants (Table 2S) are taken from ab initio calculations and scaled appropriately, as described in detail below. The Beyer−Swinehart algorithm[29] is used to evaluate the ro-vibrational density of states and the relative populations, g_i, are calculated by a Maxwell−Boltzmann distribution at 300 K. The scaled vibrational frequencies were increased and decreased by 10% to account for the range in scale factors needed to bring the calculated frequencies into agreement with the experimentally determined frequencies, as found by Pople and co-workers.[30] For the $M^+(C_6H_6)_2$ complexes with M = Na through Cs, 20% variations were applied. The uncertainty that this introduces into the analysis is included in the final uncertainties listed for the CID threshold, E_0, and the other fitting parameters.

Another consideration in the analysis of CID cross sections is whether dissociation occurs within the experimental time scale of our instrument, approximately 5×10^{-4} s in the extended dual octopole. This effect is included in our analysis by incorporating statistical theories into eq 1, as described in detail elsewhere.[26,27,31,32] This requires ro-vibrational frequencies for the energized molecules and the transition states (TSs) leading to dissociation. Because the metal−ligand interactions in the $M^+(C_6H_6)_x$ complexes are largely electrostatic (ion-induced dipole and ion-quadrupole interactions), the most appropriate model for the TS is a loose association of the ion and neutral benzene fragments. This TS is located at the centrifugal barrier for the interaction of $M^+(C_6H_6)_{x-1}$ with C_6H_6. The TS vibrations used here are the frequencies corresponding to the $M^+(C_6H_6)_{x-1}$ and C_6H_6 dissociation products, calculated as described below and listed in Table 1S. The transitional modes, those that become rotations of the completely dissociated products, are treated as rotors, a treatment that corresponds to a phase space limit (PSL), described in detail elsewhere.[31,32] For the $M^+(C_6H_6)$ complexes, there are two transitional modes, with axes perpendicular to the reaction coordinate, which are assigned as the 2-D rotor of benzene. For $M^+(C_6H_6)_2$ complexes, there are three additional transitional modes, two of which are assigned as the 2-D rotor of the $M^+(C_6H_6)$ product, again with axes perpendicular to the reaction coordinate. Of the two rotations of the dissociation products with axes parallel to the reaction coordinate, one is the third transitional mode, and the other becomes an external rotation of the TS. These rotations are taken to be the 1-D rotors of the $M^+(C_6H_6)$ and C_6H_6 products. Assignment of the external rotor and the transitional mode is unnecessary, as both modes are treated equivalently in the calculation of the kinetic rate constant. The 2-D external rotational constant of the TS is determined variationally, as detailed elsewhere,[31,32] and is treated adiabatically but with centrifugal effects included, consistent with the discussion of Waage and Rabinovitch.[33] The rotational constants of the energized molecule and the transition state for each $M^+(C_6H_6)_x$ complex are listed in Table 2S.

The form of eq 1 is expected to be appropriate for translationally driven reactions[34] and has been found to reproduce reaction cross sections well for a number of previous studies of both atom−diatom and polyatomic reactions,[35] including CID processes.[21,22,24−28,31,36−39] The model of eq 1 is convoluted with the kinetic energy distribution of the reactants, and the parameters σ_0, n, and E_0 are optimized by performing a nonlinear least-squares analysis of the data. An estimate of the error associated with the measurement of E_0 is determined from the range of threshold values obtained for different data sets with variations of the parameter n, variations associated with the ±10% or 20% uncertainties in the vibrational frequencies, the effect of increasing and decreasing the time available for the ions to dissociate (5×10^{-4} s) by a factor of 2, and the error in the absolute energy scale, ±0.05 eV (lab).

Because all sources of internal energy are included in the data analysis of eq 1, the thresholds obtained correspond to the minimum energy necessary for dissociation, in other words, the 0 K value. This assumption has been tested for several systems.[25−28] It has been shown that treating all of the ion energy (vibrational, rotational, and translational) as capable of coupling with the reaction coordinate leads to reasonable thermochemistry. The 0 K threshold energies for the CID reactions of $M^+(C_6H_6)_x$ with Xe, E_0, are converted to 0 K bond dissociation energies (BDEs), D_0, by assuming that E_0 represents the energy difference between reactants and products at 0 K.[40] This assumption requires that there are no activation barriers in excess of the bond endothermicities, which is generally true for ion−molecule reactions[35] and should be true for the simple heterolytic bond fission reactions examined here.[41]

Computational Details. Ab initio calculations were performed using Gaussian 98[42] for the alkali-metal benzene complex ions, $M^+(C_6H_6)_x$, and neutral benzene to obtain geometrical structures, vibrational frequencies, rotational constants, and energetics of dissociation of the ions. Geometry optimizations were performed first at the RHF/6-31G* level, followed by optimization at both the MP2(full)/6-31G* and the MP2(full)/6-311+G* levels for the $M^+(C_6H_6)_x$ complexes where M = Li, Na, and K. For complexes containing K^+, Rb^+, and Cs^+, the computations were performed in the same sequence

given above (RHF followed by MP2), except that the effective core potentials (ECP) and valence basis sets of Hay and Wadt were used for the description of the metal atom[43] while the 6-31G* and 6-311+G* basis sets were used for C and H atoms. As suggested by Glendening et al.,[44] a single-polarization (d) function was added to the Hay−Wadt valence basis set for K, Rb, and Cs, with exponents of 0.48, 0.24, and 0.19, respectively. Both types of calculations were performed for systems involving K^+ in order to evaluate the accuracy of the Hay−Wadt ECP/valence basis sets.

It was recently demonstrated that the MP2(full)/6-31G* level provides a reasonably good geometrical description of sodium cation complexes with various ligands.[15,45] Geometries of the benzene complexes were also optimized at the MP2(full)/6-311+G* level for comparison because we found discontinuities in the geometrical parameters of $Na^+(C_6H_6)$ and $Na^+(C_6H_6)_2$ (the details of which will be described below) compared to the results for the other mono- and bis-benzene alkali-metal ion complexes.

Vibrational frequencies and rotational constants were determined at the MP2(full)/6-31G* level for the MP2(full)/6-31G* optimized structures for all the $M^+(C_6H_6)$ complexes and $Li^+(C_6H_6)_2$. The vibrational frequencies for the $M^+(C_6H_6)_2$ complexes with M = Na, K, Rb, and Cs were estimated by scaling the calculated frequencies for $Li^+(C_6H_6)_2$ using a procedure described in detail previously.[46] The lowest frequency for the $Li^+(C_6H_6)_2$ complex was calculated to have a small negative value (-8 cm^{-1}) and corresponds to the synchronous torsional motion of the two benzene ligands about the C_6 symmetry axis. For all $M^+(C_6H_6)_2$ complexes, this motion was treated as a one-dimensional internal rotor, $I_{torsion} = I_1I_2/(I_1 + I_2)$, as described by Gilbert and Smith,[47] with a rotational constant equal to 0.19 cm^{-1}. The vibrational frequencies and rotational constants of all $M^+(C_6H_6)_x$ species are listed in Tables 1S and 2S, respectively, available in the Supporting Information. When used to model data or calculate thermal energy corrections, the MP2(full)/6-31G* calculated vibrational frequencies were scaled by a factor of 0.9646.[48]

To determine energetics, we performed single-point energy calculations at the MP2(full)/6-311+G(2d,2p) level using both the MP2(full)/6-31G* and the MP2(full)/6-311+G* optimized geometries for the Li^+, Na^+, and K^+ complexes. Calculations involving K^+, Rb^+, and Cs^+ atoms were performed at the MP2(full) level using the Hay−Wadt ECP/valence basis sets, adding the Glendening polarization (d) functions for metal atoms and the 6-311+G(2d,2p) basis set for C and H atoms. For simplicity, we term the calculations at the MP2(full)/6-311+G(2d,2p)//MP2(full)/6-31G* and MP2(full)/6-311+G(2d,2p)//MP2(full)/6-311+G* levels of theory as MP2(TZ/DZ) and MP2(TZ/TZ), respectively. For calculations of the Rb^+ and Cs^+ complexes, these designations will also be used, with the implicit understanding that ECP/valence basis sets were used for the metals. Use of an ECP/valence basis set for the metal in the $K^+(C_6H_6)_x$ calculations will be specifically noted. Basis set superposition errors (BSSE) in the calculated binding energies were estimated using the full counterpoise correction method[49] for all $M^+(C_6H_6)_x$ complexes at the MP2(TZ/DZ) level and also for M = Li and Na at the MP2(TZ/TZ) level. The BSSE corrections ranged from 4.3 kJ/mol for $K^+(C_6H_6)$ (Hay−Wadt ECP/valence basis set for K^+) to 19.5 kJ/mol for $Li^+(C_6H_6)_2$ at the MP2(TZ/DZ) level. At the MP2(TZ/TZ) level, the BSSE corrections were 10.0, 9.5, 22.7, and 14.9 kJ/mol for $Li^+(C_6H_6)$, $Na^+(C_6H_6)$, $Li^+(C_6H_6)_2$, and $Na^+(C_6H_6)_2$, respectively. These values are comparable to the BSSE corrections of 9.3, 9.8, 19.5, and 16.1 kJ/mol, respectively, calculated at the MP2(TZ/DZ) level.

Results

Collision-Induced Dissociation of $M^+(C_6H_6)_x$. Collision-induced dissociation cross sections were obtained for mono- and bis-benzene complexes of the alkali-metal cations, Li^+, Na^+, K^+, Rb^+, and Cs^+, reacting with xenon. Representative CID data are shown in Figure 1 for $Li^+(C_6H_6)$, $Cs^+(C_6H_6)$, $Li^+(C_6H_6)_2$, and $Cs^+(C_6H_6)_2$. A complete set of figures for the CID data of all other $M^+(C_6H_6)_x$ systems examined can be obtained from Figure 1S of the Supporting Information.

The dominant process observed for all systems is the loss of a single intact benzene molecule, reaction 2, over the energy ranges examined

$$M^+(C_6H_6) + Xe \rightarrow M^+ + C_6H_6 + Xe \quad (2a)$$

$$M^+(C_6H_6)_2 + Xe \rightarrow M^+(C_6H_6) + C_6H_6 + Xe \quad (2b)$$

Cross sections for the formation of M^+ from the $M^+(C_6H_6)$ complexes, reaction 2a, exhibit maxima of 4 Å^2 for $Li^+(C_6H_6)$ and 11−18 Å^2 for M = Na through Cs. The apparent thresholds for this process decrease regularly from 1.2 eV for $Li^+(C_6H_6)$ to 0.1 eV for $Cs^+(C_6H_6)$. It should be noted that the CID of $Na^+(C_6H_6)$ with Xe has been reported previously by our group.[15] The CID of this complex was repeated primarily to check the accuracy of CID experiments using the double-octopole apparatus (the previous experiment was performed on the single-octopole apparatus) and to ensure the reproducibility of our $Na^+(C_6H_6)$ BDE in light of differences with literature data.[14] In the current experiments, both the shape and magnitude of the Na^+ cross section from the $Na^+(C_6H_6)$ complex were equivalent to those reported in our previous study[15] within the quoted ±20% accuracy of absolute cross section magnitudes. This result confirms that the use of the double-octopole ion guide apparatus for CID threshold measurements of ionic metal−ligand complexes is appropriate and introduces no changes in our experimental protocol other than a longer time scale for dissociation.

For the $M^+(C_6H_6)_2$ complexes, the cross sections for the loss of a single benzene ligand, reaction 2b, reach maxima between 60 and 115 Å^2 and then begin to decline because of further dissociation of the remaining benzene ligand to form M^+. The apparent thresholds for reaction 2b decrease from 0.5 eV for $Li^+(C_6H_6)_2$ to 0.0 eV for $K^+(C_6H_6)_2$, $Rb^+(C_6H_6)_2$, and $Cs^+(C_6H_6)_2$. The cross sections for the production of $K^+(C_6H_6)$, $Rb^+(C_6H_6)$, and $Cs^+(C_6H_6)$ are nonzero at zero kinetic energy (see Figure 1d and Figure 1S of the Supporting Information). This results from the relatively low binding energies and appreciable internal energy of the bis-benzene complexes.

For the $M^+(C_6H_6)_2$ complexes, the sequential loss of two intact benzene molecules to form M^+ was observed to reach a maximum cross section of 3.3 Å^2 for $Li^+(C_6H_6)_2$ and 7−15 Å^2 for M = Na through Cs. The energy of the onset for the M^+ secondary product was found to roughly correspond to the energy at which the cross section of the primary dissociation product, $M^+(C_6H_6)$, declined. This behavior clearly indicates that the benzene molecules are lost sequentially.

As can be seen in Figure 1, the only other products observed[50] are ligand exchange reactions to form $M^+(Xe)$ and $M^+(C_6H_6)Xe$, reaction 3.

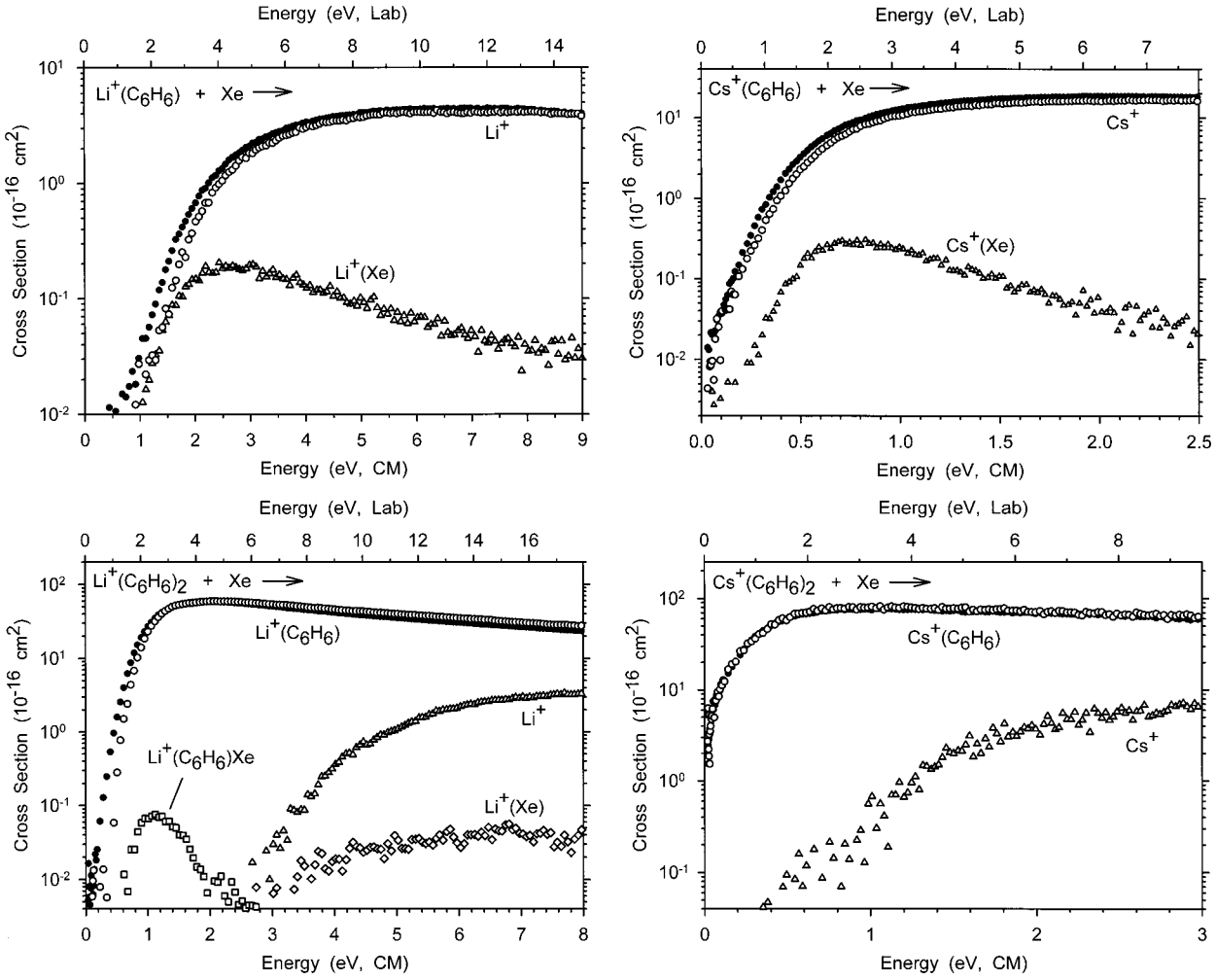

Figure 1. Cross sections for collision-induced dissociation of (a) $Li^+(C_6H_6)$, (b) $Cs^+(C_6H_6)$, (c) $Li^+(C_6H_6)_2$, and (d) $Cs^+(C_6H_6)_2$ with Xe as a function of kinetic energy in the center-of-mass frame (lower axis) and the laboratory frame (upper axis). For $M^+(C_6H_6)$ and $M^+(C_6H_6)_2$, the closed symbols represent data at a xenon pressure of ~0.2 and ~0.1 mTorr, respectively. The open symbols for all $M^+(C_6H_6)_x$ represent data extrapolated to zero pressure.

$$M^+(C_6H_6) + Xe \rightarrow M^+(Xe) + C_6H_6 \quad (3a)$$

$$M^+(C_6H_6)_2 + Xe \rightarrow M^+(C_6H_6)Xe + C_6H_6 \quad (3b)$$

$$M^+(C_6H_6)_2 + Xe \rightarrow M^+(Xe) + 2C_6H_6 \quad (3c)$$

These ligand exchange products were observed for all the systems studied except $Cs^+(C_6H_6)_2$. Reactions 3b and 3c probably occur in this system, but because the intensity of the primary beam was low, these product channels were not collected. The apparent thresholds for the $M^+(Xe)$ and $M^+(C_6H_6)Xe$ ligand exchange products from the CID of $M^+(C_6H_6)$ and $M^+(C_6H_6)_2$, respectively, are near those of the primary dissociation products, M^+ and $M^+(C_6H_6)$, respectively. The thermodynamic thresholds of these channels must be lower than those of the primary dissociation by the M^+-Xe and $M^+(C_6H_6)-Xe$ binding energies, respectively.[51] This is not always evident in the apparent thresholds because of the large difference in the relative magnitudes of these channels.

In the CID of the $M^+(C_6H_6)$ complexes, the cross sections for the $M^+(Xe)$ product were observed to have maximum magnitudes between 0.2 and 0.9 Å^2. The cross sections begin to decline rapidly at somewhat higher energies because the product decomposes to $M^+ + Xe$. Compared to these processes, the cross sections for the $M^+(C_6H_6)Xe$ product in the CID of the $M^+(C_6H_6)_2$ complexes have maximum magnitudes about 1 order of magnitude smaller. These cross sections also begin to decline rapidly after reaching their maxima because they dissociate to $M^+(C_6H_6) + Xe$. Loss of C_6H_6 to form $M^+(Xe)$ is also possible but is a higher-energy process. The cross sections for the $M^+(Xe)$ product in the CID of the $M^+(C_6H_6)_2$ complexes reach maximum values between 0.05 and 0.4 Å^2 and decline as the M^+ cross sections grow in.

It is possible that the ligand exchange reactions represented in reactions 3a and 3b could cause competitive shifts in the observed thresholds for the primary dissociation products. This competition is unlikely to have an appreciable affect (smaller than the reported experimental error limits) on the primary dissociation threshold measurements of the current systems because their cross section magnitudes are at least 1 order of magnitude smaller than those of the primary product ion for all $M^+(C_6H_6)$ systems and at least 2 orders of magnitude smaller for all $M^+(C_6H_6)_2$ systems. Several other reasons have been discussed in detail elsewhere.[52] As little systematic and reliable information can be obtained from the cross sections for these ligand exchange products, they will not be discussed further.

Thermochemical Results. Previous CID studies using guided ion beam mass spectrometry[24,25,27,53] have shown that the best measure of bond dissociation energies for metal−ligand complex ions comes from the analysis of the cross sections for the primary dissociation products, reaction 2 in the current

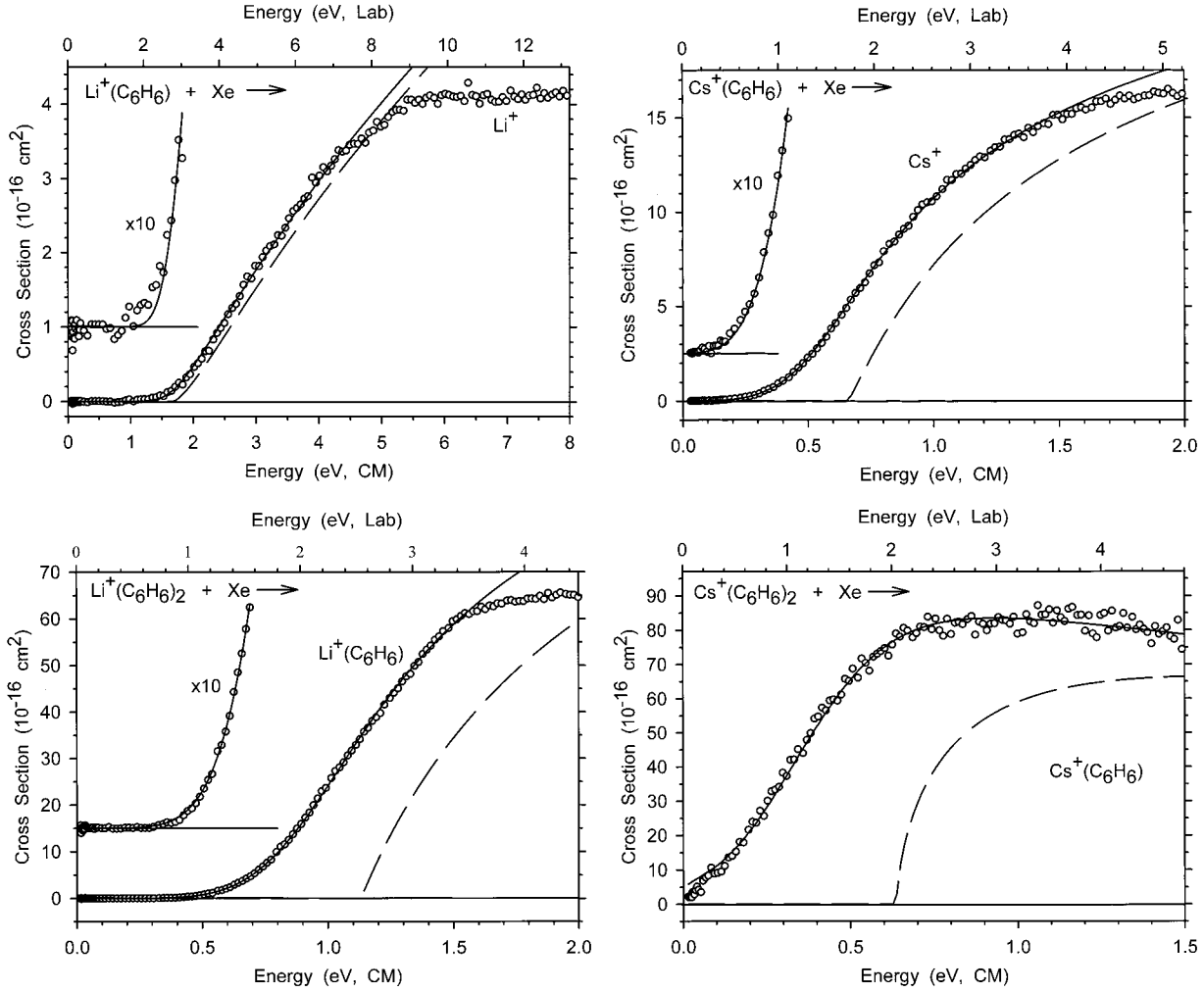

Figure 2. Zero pressure extrapolated cross sections for the primary collision-induced dissociation processes of (a) $Li^+(C_6H_6)$, (b) $Cs^+(C_6H_6)$, (c) $Li^+(C_6H_6)_2$, and (d) $Cs^+(C_6H_6)_2$ with Xe in the threshold region as a function of kinetic energy in the center-of-mass frame (lower axis) and the laboratory frame (upper axis). Solid lines show the best fits to the data using the model of eq 1 convoluted over the neutral and ion kinetic energies and the internal energy distributions of the ions. Dashed lines show the model cross sections in the absence of experimental kinetic energy broadening for reactants with an internal energy of 0 K. In parts a−c, the data and models expanded by a factor of 10 and offset from zero are also shown.

$M^+(C_6H_6)_x$ systems. Therefore, only these CID processes were analyzed using eq 1. The results of these analyses are listed in Table 1 for all $M^+(C_6H_6)_x$ systems, and the representative fits using eq 1 for $Li^+(C_6H_6)$, $Cs^+(C_6H_6)$, $Li^+(C_6H_6)_2$, and $Cs^+(C_6H_6)_2$ are shown in Figure 2. The representative fits using eq 1 for all other $M^+(C_6H_6)_x$ complexes are given in Figure 2S, available in the Supporting Information. Experimental cross sections for the primary dissociation processes of the $M^+(C_6H_6)_x$ complexes are accurately reproduced over energy ranges that exceed 1 eV in all cases and over cross section magnitudes of a factor of at least 100 for all complexes except $Rb^+(C_6H_6)_2$ and $Cs^+(C_6H_6)_2$. For these two systems, only a factor of 10 in magnitude is available in the data as a result of the nonzero cross section magnitudes for the product ions at zero kinetic energy. In the analysis of the cross sections using eq 1 for $K^+(C_6H_6)_2$, $Rb^+(C_6H_6)_2$, and $Cs^+(C_6H_6)_2$, the lowest energy data points (below 0.1 eV) were not included, as can be seen in Figure 2d for $Cs^+(C_6H_6)_2$ and Figure 2S for $K^+(C_6H_6)_2$ and $Rb^+(C_6H_6)_2$. The deviations at low energies are believed to be a result of metastable ions in the $M^+(C_6H_6)_2$ ion beams, which lead to a depletion of $M^+(C_6H_6)$ product intensity at these low kinetic energies. Even so, the data are still reproduced reasonably well in these low-energy regions.

As mentioned above, the effect of kinetic shifts on the CID thresholds was examined using an RRKM treatment with a loose phase space limit (PSL) model for the dissociation transition state. Previous studies have demonstrated that this model provides the most accurate determination of the magnitude of kinetic shifts for CID processes of metal−ligand complexes.[21,22,31,32,36−39,52] As is evident by an examination of Table 1, the kinetic shifts for the present systems were found to be very small, ranging from 0 to 0.03 eV. Even though the number of vibrational modes is fairly high for these complexes, 33 for $M^+(C_6H_6)$ and 69 for $M^+(C_6H_6)_2$, the low magnitude of the kinetic shifts is understandable because the bond dissociation energies for these complexes are fairly low.

A general measure of the looseness of the transition state is reflected in the entropies of activation, $\Delta S^{\ddagger}$, listed in Table 1 at 1000 K. The magnitudes of $\Delta S^{\ddagger}_{1000}$ calculated in this study are comparable to those determined by Lifshitz, 29−46 J K^{-1} mol^{-1}, for several simple ionic bond cleavage dissociation reactions,[54] although slightly higher in the case of $M^+(C_6H_6)_2$. The $\Delta S^{\ddagger}_{1000}$ values for the dissociation of the $M^+(C_6H_6)_2$ complexes increase as the dissociation threshold decreases on going from $Li^+(C_6H_6)_2$ to $Cs^+(C_6H_6)_2$. This seems sensible and implies that the transition state is getting looser. For the $M^+(C_6H_6)$ complexes, however, the trend is contrary to that intuitively expected, with $\Delta S^{\ddagger}_{1000}$ decreasing as the dissociation threshold decreases on going from $Li^+(C_6H_6)$ to $Cs^+(C_6H_6)$. Closer analysis shows that, while the rotational contribution to the entropy of activation is

TABLE 3: Experimental and Calculated $M^+(C_6H_6)_x$ Bond Dissociation Energies (in kJ/mol) at 0 K

			theory							
	experiment		D_0 (TZ/DZ)[a,c]		D_0 (TZ/DZ)[a,d]		literature			
bond	GIBMS[a]	literature[b]	no BSSE	BSSE	no BSSE	BSSE	MP2[e]	SVWN[f]	BP86[g]	CBS[h]
$Li^+-C_6H_6$	161.1 (13.5)	151.9 (8.0)[i]	152.6	143.3	153.5	143.5	143.5	159.4	138.1	151.0 (0.8)
$Na^+-C_6H_6$	92.6 (5.8)	115.8 (6.3)[j]	99.1	89.4	99.4	89.9	87.9	110.4	87.0	102.1 (1.2)
	88.3 (4.3)[k]						90.4[l]			
$K^+-C_6H_6$	73.3 (3.8)	76.2 (6)[m]	76.9	71.5	77.0			76.6	54.4	83.7 (1.7)
			71.3[n]	67.0[n]	71.4[n]		67.4			
$Rb^+-C_6H_6$	68.5 (3.8)		60.3[n]	53.2[n]	62.7[n]		55.6	65.7	46.0	68.2 (0.8)
$Cs^+-C_6H_6$	64.6 (4.8)		55.3[n]	47.7[n]	55.5[n]		48.5	56.9	37.6	51.9 (0.8)
$(C_6H_6)Li^+-C_6H_6$	104.2 (6.8)		127.7	108.2	127.1	104.5				
$(C_6H_6)Na^+-C_6H_6$	80.0 (5.8)		87.9	71.8	88.0	73.1				
$(C_6H_6)K^+-C_6H_6$	67.5 (6.8)	71.0 (6)[m]	65.7	56.1	65.6					
			61.6[n]	53.1[n]	61.7[n]					
$(C_6H_6)Rb^+-C_6H_6$	62.7 (7.7)		62.0[n]	45.8[n]	60.9[n]					
$(C_6H_6)Cs^+-C_6H_6$	58.8 (7.7)		48.5[n]	36.2[n]	49.1[n]					

[a] Present results. Uncertainties in parentheses. [b] All literature values adjusted to 0 K, as described in text. Uncertainties in parentheses. [c] MP2(full)/6-311+G(2d,2p)//MP2(full)/6-31G*; corrected for zero-point energies. [d] MP2(full)/6-311+G(2d,2p)//MP2(full)/6-311+G*; corrected for zero-point energies. [e] Ref 69, MP2(FC)/6-311+G*//MP2(FC)/6-311+G*; corrected for zero-point energies and BSSE. Hay−Wadt ECP/valence basis set for K^+, Rb^+, Cs^+. [f] Ref 69, SWVN/TZ94p; uncorrected for BSSE. Hay−Wadt ECP/valence basis set for Rb^+ and Cs^+. [g] Ref 69, BP86/TZ94p; uncorrected for BSSE. Hay−Wadt ECP/valence basis set for Rb^+ and Cs^+. [h] Ref 70, MP2 complete basis set (CBS) extrapolations using aug-cc-pVxZ, x = D, T, and Q, with core/valence and CCSD(T) corrections. Hay−Wadt ECP used for Rb^+ and Cs^+ core electrons. Uncertainties in parentheses. [i] Ref 12. [j] Ref 14. [k] Value obtained in previous CID work, ref 15. [l] MP2(full)/6-311+G*//MP2(full)/6-311+G*. [m] Ref 16. [n] Hay−Wadt ECP/valence basis set for the metal atom, as described in the text.

approximately constant, the vibrational contribution becomes a larger negative number as the metal is changed from Li^+ to Cs^+ for the $M^+(C_6H_6)$ complexes. This is because the metal−ligand frequencies decrease as the metal gets heavier (see Table 1S). This type of behavior has been observed in a previous study involving Li^+, Na^+, and K^+ complexes with several azoles[55] and is most likely a general trend for different alkali-metal ions bound to a single ligand.

It should be noted that the magnitudes of $\Delta S^{\ddagger}_{1000}$ listed in Table 1 were determined by treating the transitional modes of the $M^+(C_6H_6)_x$ transition state (i.e., dissociated products in the PSL model) with axes perpendicular to the reaction coordinate as 2-D internal rotors (see Table 2S), consistent with other recent studies.[15,56] In previous studies utilizing the PSL model,[21,22,31,32,36−39,46,55] these perpendicular transitional modes were described as two 1-D internal rotors, even those that would typically be considered as 2-D rotations of the free ligands, assuming that the free ligands can be approximated as symmetric tops. For systems with small kinetic shifts, such as the current $M^+(C_6H_6)_x$ systems, the only difference in the results between the two treatments will be an increase of $R \ln \pi$ (9.5 J K^{-1} mol^{-1}) in the magnitude of $\Delta S^{\ddagger}_{1000}$ for every 2-D internal rotor that is treated as two 1-D internal rotors in the dissociation products. In the present systems, this would amount to increases of 9.5 and 19.0 J K^{-1} mol^{-1} for $M^+(C_6H_6)$ and $M^+(C_6H_6)_2$, respectively, between the values of $\Delta S^{\ddagger}_{1000}$ calculated using the current and previous methods. For systems with a significant kinetic shift, there may also be a change in the predicted magnitude of the kinetic shift between the two treatments because the RRKM rate constant will change by a factor of π for every 2-D internal rotor in the dissociated products.[57] We presently believe that using the 2-D rotors is more appropriate, and work is currently in progress to verify this.

In a previous report concerning the BDEs of $Na^+(L)$ complexes,[15] a value of 50 J K^{-1} mol^{-1} was reported for the $\Delta S^{\ddagger}_{1000}$ of $Na^+(C_6H_6)$, which differs slightly from the currently reported value in Table 3, 43 J K^{-1} mol^{-1}. Both studies treat the perpendicular internal rotations as a 2-D internal rotor, and the difference in $\Delta S^{\ddagger}_{1000}$ values results from differences in reaction degeneracies, 1.0 and 0.5 in the former and present studies, respectively. For systems in which there is no optical isomerism, the reaction degeneracy is given by the ratio of rotational symmetry numbers of the energized molecule and transition state.[47] In the PSL model, which assumes that the transition state is represented by the fully dissociated products, a reaction degeneracy of 0.5 is the correct value for the dissociation of $Na^+(C_6H_6)$, given the rotational symmetry numbers of 6 and 12 for $Na^+(C_6H_6)$ and C_6H_6, respectively.[58] This difference in reaction degeneracy only affects the magnitude of $\Delta S^{\ddagger}_{1000}$ and not the value of the threshold energy because the kinetic shift is negligible for $Na^+(C_6H_6)$.

Theoretical Results. Energy optimized structures for all $M^+(C_6H_6)_x$ complexes were calculated as described above. The geometrical parameters of these optimized structures determined at the MP2(full)/6-31G* and the MP2(full)/6-311+G* levels are given in Table 2. The most stable structures for $M^+(C_6H_6)$ and $M^+(C_6H_6)_2$ were those with C_{6v} and D_{6h} symmetries, respectively. These symmetrical structures are displayed in Figure 3 for the $Li^+(C_6H_6)$ and $Li^+(C_6H_6)_2$ complexes calculated at the MP2(full)/6-31G* level of theory.

As can be seen in Table 2, the calculations predict that the metal carbon and therefore the metal ring-centroid distances[59] increase as the metal is changed from Li^+ to Cs^+ for both the $M^+(C_6H_6)$ and $M^+(C_6H_6)_2$ complexes at both levels of theory. The use of the Hay−Wadt ECP/valence basis set for K^+ in the $K^+(C_6H_6)_x$ complexes resulted in increases of the metal−carbon and metal−centroid distances by an average of 0.027 and 0.081 Å, respectively, compared to the distances calculated when the 6-31G* and the 6-311+G* basis sets were used for all atoms. The metal−carbon and metal−centroid distances increased at the MP2(full)/6-31G* level as the second benzene was added to $M^+(C_6H_6)$, as expected for electrostatically bound complexes, except when the metal was Na^+. At the MP2(full)/6-311+G* level, these distances were found to increase for Li^+, Na^+, and K^+, but decreased for Rb^+ and Cs^+, from one to two benzene rings in the complex. The calculations for the $K^+(C_6H_6)_x$ complexes using the Hay−Wadt ECP/valence basis set followed the same trends and possessed similar magnitudes for the differences in distances between the mono- and bis-benzene complexes as was predicted for the all-electron calculations.

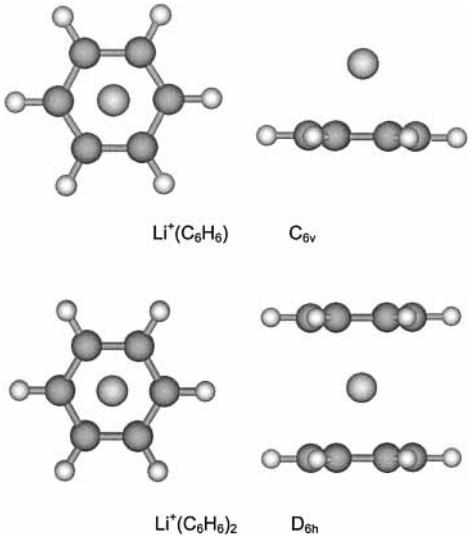

Figure 3. Ground-state geometries of the $Li^+(C_6H_6)$ (upper) and $Li^+(C_6H_6)_2$ (lower) complexes viewed from the side and from above, optimized at the MP2(full)/6-31G* level of theory.

The unexpected decreases in the metal−carbon and metal−centroid distances for $Na^+(C_6H_6)_x$, $Rb^+(C_6H_6)_x$, and $Cs^+(C_6H_6)_x$ probably reflect slight inaccuracies in the ability of the theoretical methods used here to describe the subtle bonding changes that are occurring in the bis-benzene complexes compared to those in the monobenzene complexes. However, it is interesting to note that the metal−centroid distance calculated for $Cs^+(C_6H_6)_2$ (∼3.4 Å) is fairly close to an experimentally determined metal−centroid distance (3.57 Å) for a cesium complex of *p-tert*-butylcalix[4]arene.[5]

The C−C bond lengths in the benzene rings were found to increase very slightly for the metal complexes (<0.010 Å) compared to those for the free ligand (Table 2). The largest effect of the metal ion on the benzene ring structure is the bending of the hydrogen atoms out of the plane of the benzene ring and away from the metal ion. The magnitude of this bending is predicted to be the smallest for the Li^+ complexes and generally increases as the size of the metal ion is increased at both levels of theory. Also, the bending is smaller for the bis-benzene complexes than for the monobenzene systems.

An optimization was also performed for $Na^+(C_6H_6)_2$ at the MP2(full)/6-31G* level, in which the symmetry was fixed in the D_{6d} point group (the staggered orientation with the benzene rings rotated 30° from one another) but all other degrees of freedom were allowed to vary. This optimized structure was found to have exactly the same geometrical parameters as those listed in Table 2 for the $Na^+(C_6H_6)_2$ D_{6h} structure and an energy that was slightly higher by 0.0008 kJ/mol but essentially equivalent to that of the D_{6h} structure at the MP2(full)/6-31G* level. A single-point calculation at the MP2(full)/6-311+G(2d,-2p) level (not corrected for zero-point energy or BSSE) at the MP2(full)/6-31G* optimized D_{6d} geometry indicated that this structure was lower in energy than that of the D_{6h} structure by 0.10 kJ/mol. Given that the energy difference between these structures at the MP2(TZ/DZ) level is well below the accuracy of the computational methods, the two structures are energetically equivalent. These results corroborate the assignment of the lowest calculated vibrational frequency of the $M^+(C_6H_6)_2$ complexes as corresponding to an unhindered torsional motion of the benzene rings about the C_6 symmetry axis.

Theoretical values of the BDEs of the $M^+(C_6H_6)_x$ complexes were determined using both the MP2(full)/6-31G* and the MP2-(full)/6-311+G* geometries and single-point energy calculations at the MP2(full)/6-311+G(2d,2p) level. These results are listed in Table 3 along with the current experimental determinations. The values determined at the MP2(TZ/DZ) level were corrected for zero-point energies (ZPEs) and BSSE for all $M^+(C_6H_6)_x$ complexes. The BDEs calculated at the MP2(TZ/TZ) level were corrected for ZPEs for all $M^+(C_6H_6)_x$ complexes but corrected for BSSE only for the $Li^+(C_6H_6)$, $Na^+(C_6H_6)$, $Li^+(C_6H_6)_2$, and $Na^+(C_6H_6)_2$ complexes. The single-point energy calculations involving the MP2(full)/6-311+G* optimized geometries were primarily performed in order to determine if the differences in the calculated metal−carbon and metal−centroid distances described above would affect the theoretical BDEs. As can be seen from an examination of Table 3, the BDEs calculated using the two different optimized geometries are essentially identical, with a mean absolute deviation (MAD) of only 0.6 ± 0.7 kJ/mol for the 12 values without BSSE correction. The agreement between the four BDEs where BSSE was included is also excellent with a MAD of 1.4 ± 1.6 kJ/mol. Given the good agreement observed between the BDEs using the two optimized geometries and the relatively large amount of computational time that would be required to perform the calculations at the MP2(TZ/TZ) level, BSSE corrections were not performed for the larger complexes. Also, to simplify the following discussion, we will make comparisons to the theoretical values with the ZPE- and BSSE-corrected MP2(TZ/DZ) BDEs and the ZPE-corrected, but not BSSE-corrected, MP2(TZ/TZ) BDEs. These BDEs shall be referred to as the MP2(TZ/DZ)BSSE and MP2-(TZ/TZ)NoBSSE values, respectively.

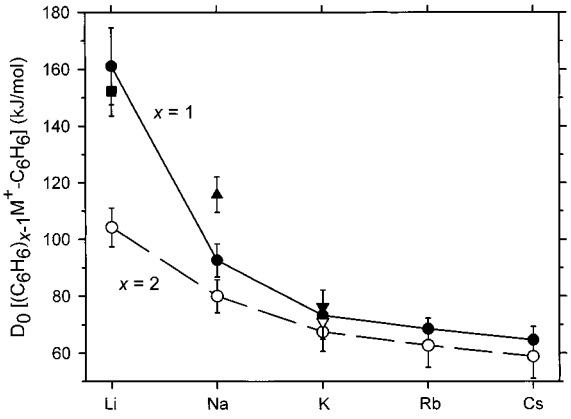

Figure 4. Bond dissociation energies at 0 K for the mono-benzene (closed symbols) and bis-benzene (open symbols) complexes of the alkali-metal ions. The plot shows results from the present experimental work (circles, Table 3), Woodin and Beauchamp (square, ref 12), Castleman and co-workers (triangle, ref 14), and Kebarle and co-workers (inverted triangles, ref 16).

Discussion

Trends in Experimental $M^+(C_6H_6)_x$ Bond Dissociation Energies. The 0 K experimental BDEs of the $M^+(C_6H_6)_x$ complexes are listed in Table 3 and pictorially represented in Figure 4. Both the $M^+-C_6H_6$ and $(C_6H_6)M^+-C_6H_6$ BDEs are found to decrease monotonically as the metal is changed from Li^+ to Cs^+. This is the expected trend for a bonding scheme based primarily on electrostatic interactions (ion-induced dipole and ion−quadrupole)[4] because the increasing size of the ion[60] leads to inherently increasing metal−ligand bond distances (see Table 2). Also, the difference in BDEs for adjacent metals becomes smaller as the metal ion is changed from Li^+ to Cs^+ for both the $M^+(C_6H_6)$ and $M^+(C_6H_6)_2$ complexes. This results from a combination of two factors: the relative changes in ionic

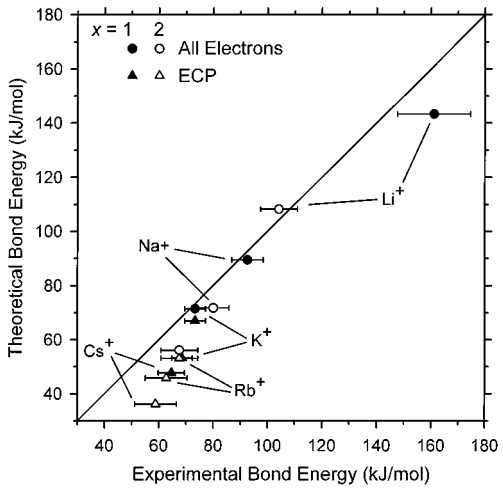

Figure 5. Theoretical vs experimental bond dissociation energies at 0 K for the mono-benzene (closed symbols) and bis-benzene (open symbols) complexes of the alkali-metal ions. All values are taken from Table 3. The theory is represented by the present calculations at the MP2(full)/6-311+G(2d,2p)//MP2(full)/6-31G* level for all electron calculations (circles) and with the use of the Hay−Wadt ECP and valence basis set for the K, Rb, and Cs metal ions (triangles). The diagonal line indicates the values for which calculated and measured bond dissociation energies are equal.

radii for the alkali-metal cations becomes smaller,[60] and the nonlinear distance dependencies of the electrostatic interactions fall off rapidly as r^{-3} and r^{-4} for the ion−quadrupole and ion-induced dipole interactions, respectively.

The $(C_6H_6)M^+-C_6H_6$ BDE compared to the $M^+-C_6H_6$ BDE is smaller for M = Li and reaches a nearly constant value for M = K through Cs. In a recent study involving the trends in BDEs for $Li^+-[O(CH_3)_2]_x$ complexes,[21] it was suggested that such a trend is primarily due to Coulombic and dipole−dipole repulsions between the ligands. Using the M^+−centroid distances in Table 2, we calculate the distance between the benzene rings to be ∼3.90 Å in $Li^+(C_6H_6)_2$, whereas this distance increases to 6.8 Å in $Cs^+(C_6H_6)_2$. Clearly, the magnitude of the repulsive ligand−ligand interactions for $Li^+(C_6H_6)_2$ will be larger than those of the other $M^+(C_6H_6)_x$ complexes, leading to a $(C_6H_6)Li^+-C_6H_6$ bond weaker than the $Li^+-C_6H_6$ bond. The constancy of the changes in sequential $M^+(C_6H_6)_x$ BDEs when M = K through Cs suggests that the magnitude of the ligand−ligand interactions are comparable in these systems.

Comparison of Experimental and Theoretical $M^+(C_6H_6)_x$ Bond Dissociation Energies. The theoretically calculated $M^+(C_6H_6)_x$ BDEs are listed in Table 3, and the comparison between the experimental BDEs and theoretical values at the MP2(TZ/DZ) level is shown in Figure 5. In general, the theoretical calculations are in qualitative agreement with the observed experimental trends in BDEs discussed above. Both find that the primary BDEs decrease monotonically as the metal is changed from Li^+ to Cs^+ for the $M^+(C_6H_6)_x$ complexes. Also, the calculations predict that the difference in sequential BDEs is largest for the species containing Li^+ and gradually becomes smaller as the size of the metal ion increases.

Quantitatively, the agreement between the six experimental BDEs and the theoretical $M^+(C_6H_6)_x$ (x = 1 and 2) BDEs calculated including all electrons (M = Li, Na, K) is reasonably good, with a mean absolute deviation (MAD) of 7.7 ± 6.1 kJ/mol for the MP2(TZ/DZ)BSSE BDEs (six values) and 8.5 ± 7.5 kJ/mol for the MP2(TZ/TZ)NoBSSE BDEs (six values). The low MP2(TZ/DZ)BSSE BDE for $Li^+(C_6H_6)$ compared to the experimental value (difference of 17.8 kJ/mol) is disappointing. Given that Li^+ has the least number of electrons of all the alkali metals, the theoretical description of compounds containing Li^+ might be expected to be fairly accurate. However, Li^+ possesses the most covalent character in its bonding to benzene. This is shown by the calculated partial charge on M^+: 0.77 for Li^+-(C_6H_6) compared to ∼0.9−1.0 for all other $M^+(C_6H_6)$ at the MP2(TZ/DZ) level. Hence, higher levels of theory may be required to describe this complex accurately, a conclusion we also reached for Li^+ complexes with the nucleic acid bases uracil, thymine, and adenine.[61]

The agreement between the experimental BDEs and the theoretical values calculated using the Hay−Wadt ECP/valence basis set for the metal atoms (K, Rb, and Cs) is not as good, with a MAD of 14.1 ± 5.8 kJ/mol at the MP2(TZ/DZ)BSSE level (six values). For the MP2(TZ/TZ)NoBSSE BDEs (six values), the agreement between experiment and theory using the ECPs is improved, with a MAD of 5.7 ± 3.4 kJ/mol. It is clear from Table 3 and Figure 5 that the calculated values using the Hay−Wadt ECP/valence basis sets, both with and without BSSE corrections, are all low compared the experimental values and that the deviations become worse as the metal becomes heavier. A comparison of the theoretical BDEs for the $K^+(C_6H_6)_x$ complexes calculated with all electrons and using the ECP shows that the failure to include all electrons lowers the calculated BDE. These observations suggest that systematic inaccuracies are introduced by the use of ECP/valence basis sets for the computation of the BDEs of alkali-metal cations with benzene.

In general, the theoretical results imply that the current theory levels are inadequate for an accurate description of the bonding between the heavier alkali-metal ions and the diffuse π cloud of benzene in both the $M^+(C_6H_6)$ and $M^+(C_6H_6)_2$ complexes. Also, in light of the possibility that the counterpoise correction method may overestimate the magnitude of BSSE,[62−64] it may be more appropriate to consider the MP2(TZ/TZ)NoBSSE and the MP2(TZ/DZ)BSSE BDEs as upper and lower limits, respectively.

We have considered the possibility that our experimental BDEs for complexes with the heavy alkali metals (Rb^+ and Cs^+) are too high. To check this, we modeled the CID cross sections for the Rb^+ and Cs^+ complexes using eq 1, but with E_0 fixed at the value of the theoretically calculated BDE and allowing the parameters σ_0 and n to optimize. The protocol established in our laboratory is to model and reproduce the data using eq 1 over as large an energy range as possible while simultaneously maintaining a good fit to the data in the threshold region. To obtain fits which satisfactorily reproduced the data in the threshold region and in which E_0 was fixed at the calculated BDEs, we had to reduce the energy ranges considerably compared to the energy ranges shown in Figures 2 and 2S. Concomitantly, the value of the parameter n was found to increase by approximately a factor of 2 compared to the values listed in Table 1. Allowing E_0, σ_0, and n to reoptimize from the values of these fixed E_0 fits over the reduced energy ranges generally resulted in a return to higher values of E_0 and lower values of n. From these results and from the quality of the fits shown in Figures 2 and 2S, we believe that the BDEs for the Rb^+ and Cs^+ complexes with benzene determined here are accurate and lower values outside our quoted error limits are inconsistent with the data.

Conversion from 0 to 298 K. To allow comparison to some of the previous literature values and commonly used experimental conditions, we convert the 0 K bond energies determined

TABLE 4: Enthalpies and Free Energies (in kJ/mol)[a] for $M^+(C_6H_6)_x$ at 0 and 298 K

system	ΔH_0[b]	$\Delta H_{298} - \Delta H_0$[c]	ΔH_{298}	$T\Delta S_{298}$[c]	ΔG_{298}
$Li^+(C_6H_6)$	161.1 (13.5)	3.3 (2.0)	164.4 (13.6)	32.2 (4.4)	132.2 (14.3)
$Na^+(C_6H_6)$	92.6 (5.8)	1.7 (1.8)	94.3 (6.1)	30.5 (5.5)	63.8 (8.2)
$K^+(C_6H_6)$	73.3 (3.8)	0.9 (1.5)	74.2 (4.1)	28.3 (5.8)	45.9 (7.1)
$Rb^+(C_6H_6)$	68.5 (3.8)	0.3 (1.3)	68.8 (4.0)	26.5 (6.0)	42.3 (7.2)
$Cs^+(C_6H_6)$	64.6 (4.8)	0.1 (1.2)	64.7 (4.9)	25.8 (6.0)	38.9 (7.7)
$Li^+(C_6H_6)_2$	104.2 (6.8)	−0.5 (2.0)	103.7 (7.1)	39.6 (9.5)	64.1 (11.9)
$Na^+(C_6H_6)_2$	80.0 (5.8)	0.3 (2.1)	80.3 (6.2)	41.5 (8.9)	38.8 (10.8)
$K^+(C_6H_6)_2$	67.5 (6.8)	0.7 (2.2)	68.2 (7.1)	42.9 (8.9)	25.3 (11.4)
$Rb^+(C_6H_6)_2$	62.7 (7.7)	0.6 (2.2)	63.3 (8.0)	43.6 (9.0)	19.7 (12.0)
$Cs^+(C_6H_6)_2$	58.8 (7.7)	0.5 (2.2)	59.3 (8.0)	43.9 (9.1)	15.4 (12.1)

[a] Uncertainties in parentheses. [b] Present experimental results (Table 3). [c] Calculated using standard formulas and molecular constants determined at the MP2(full)/6-31G* level, except those for $M^+(C_6H_6)_2$ where M = Na through Cs, which were determined using the calculated $Li^+(C_6H_6)_2$ frequencies and a relative scaling procedure described in the text. The molecular constants for all $M^+(C_6H_6)_x$ complexes are given in Tables S1 and S2. Uncertainties correspond to increases and decreases in the metal−ligand frequencies by a factor of 2 and ±10% variations in the benzene vibrational frequencies.

here to 298 K bond enthalpies and free energies. The enthalpy conversions and the entropies are calculated using a rigid rotor/harmonic oscillator approximation and molecular constants calculated at the MP2(full)/6-31G* level (Tables 1S and 2S). Table 4 lists the 298 K enthalpies, free energies, and enthalpic and entropic corrections along with the 0 K enthalpies for systems examined here. The uncertainties in these values are determined by increasing and decreasing the metal−ligand frequencies by a factor of 2 and ±10% variations in the benzene frequencies for all $M^+(C_6H_6)_x$ complexes. Overall, the enthalpy and entropy corrections and the derived ΔG_{298} values listed in Table 4 should be viewed as first approximations.

Comparison with Experimental Literature Values. For most of the alkali-metal benzene complexes examined in the present work, there are no previous experimental determinations of the binding energies. Previous experimental values have been reported for $Na^+(C_6H_6)$[14] and $K^+(C_6H_6)_x$ (x = 1 and 2),[16] determined in high-pressure mass spectrometry (HPMS) experiments. For $Li^+(C_6H_6)$, there are two previous experimental studies in which the relative free energy of binding was measured using ion cyclotron resonance (ICR) mass spectrometry.[12,13] For these previous experimental values to be compared to the present experimental 0 K bond enthalpies, various temperatures conversions and other corrective factors need to be applied.

The previous experimental values of the bond enthalpy of $Na^+(C_6H_6)$ was reported by Castleman and co-workers as 117.2 ± 6.3 kJ/mol,[14] and Kebarle and co-workers reported 76.6 and 71.1 kJ/mol for $K^+(C_6H_6)$ and $K^+(C_6H_6)_2$, respectively.[16] These values were determined from the slope of van't Hoff plots for metal ion−benzene equilibria using HPMS. Kebarle and co-workers did not report error limits for the $K^+(C_6H_6)$ and $K^+(C_6H_6)_2$ bond enthalpies, but an estimate (6 kJ/mol) can be taken from the error in the $Na^+(C_6H_6)$ bond enthalpy reported by Castleman and co-workers. To convert these ΔH values to ΔH_0 values, it is appropriate to consider the average of the experimental temperature range as the representative temperature for the reported enthalpy change: 600, 500, and 400 K for $Na^+(C_6H_6)$, $K^+(C_6H_6)$, and $K^+(C_6H_6)_2$, respectively. Accordingly, the literature ΔH_0 values reported in Table 3 and displayed in Figure 4 were obtained by subtracting 1.4, 0.4, and 0.1 kJ/mol, respectively, from the reported ΔH values.[65]

Woodin and Beauchamp (WB)[12] reported an absolute free energy of binding of 124.3 ± 8.4 kJ/mol at 298 K, while Taft and co-workers[13] reported an identical value of 124.3 ± 8.4 kJ/mol at 373 K. Both of these experimental studies used ICR mass spectrometry to measure the relative free energies of Li^+ binding with neutral ligands, including benzene, which were then converted to absolute free energies of binding by the use of anchor values whose absolute free energy of binding was known. Because these values are essentially equivalent (the final 0 K BDEs derived from these studies differ by less than 1 kJ/mol), only the value of WB will be discussed further.

WB used the $\Delta G_{298}[Li^+(H_2O)]$ value reported by Dzidic and Kebarle,[66] which was actually an extrapolated value based on the measured values for $Li^+(H_2O)_x$ (x = 2−5) as an absolute anchor. A direct measurement of $\Delta H_{298}[Li^+(H_2O)]$ in our laboratory[37,67] finds that the $\Delta G_{298}[Li^+(H_2O)]$ reported by Dzidic and Kebarle is slightly too high by 3.0 kJ/mol. Adjusting $\Delta G_{298}[Li^+(C_6H_6)]$ for this revision and using the value of $T\Delta S_{298}[Li^+(C_6H_6)]$ given in Table 4 (comparable to the value estimated by WB), we obtain a revised estimate of 155.2 ± 8.0 kJ/mol for $\Delta H_{298}[Li^+(C_6H_6)]$ (WB reported 158.6 ± 8.4 kJ/mol). Using the enthalpy correction given in Table 4, we can then convert this revised 298 K bond enthalpy to a 0 K value, as listed in Table 3 and shown in Figure 4.

As can be seen from Figure 4 and Table 3, the agreement between the present results and the previous experimental determinations is quite good for $Li^+(C_6H_6)$, $K^+(C_6H_6)$, and $K^+(C_6H_6)_2$, with deviations that are within the experimental errors (MAD of 5.2 ± 3.5 kJ/mol for the three values). The agreement between the current and previous experimental $Na^+(C_6H_6)$ BDE is, however, quite poor, as previously discussed.[15] Although the exact reason for the apparently systematic deviations is unclear, one possibility is the presence of Na atoms with electrons in high Rydberg states, formed in the thermionic emission source, which autoionize upon complexation with the neutral ligand.[68] This would artificially shift the equilibrium toward the $Na^+(C_6H_6)$ complex side and result in a higher apparent bond enthalpy for the complex.

Comparison with Theoretical Literature Values. There have been a number of previous ab initio theoretical studies of the binding energies of various alkali-ion mono-benzene complexes, $M^+(C_6H_6)$, most of which were performed using basis sets of double-ζ quality at the RHF and MP2 levels. The details and results from all of these different studies will not be discussed in detail here, but the reader is referred to the review article of Ma and Dougherty[4] for a complete listing. Also, in a previous report on $Na^+(L)$ binding energies from our laboratory,[15] a series of theoretical calculations were performed for the $Na^+(C_6H_6)$ complex, which include MP2 (equivalent to the current method) calculations, DFT (B3LYP and B3P86) calculations, and various compound methods (CBS-4, CBS-4M, CBS-Q, and G2), and the reader is referred to that paper for a discussion of these results. The most extensive theoretical calculations concerning the BDEs of the alkali-metal cation−

monobenzene complexes are the studies of Nicholas et al.[69] and Feller et al.[64,70]

In the study of Nicholas et al.,[69] BDEs corrected for ZPE and BSSE for the $M^+(C_6H_6)$ complexes (M = Li through Cs) were calculated at the MP2(FC)/6-311+G*//MP2(FC)/6-311+G* level of theory, and they used the Hay−Wadt ECP/valence basis sets for K^+, Rb^+, and Cs^+. In addition, they performed calculations using density functional theory (DFT) at the local (SVWN/TZ94p) and nonlocal (BP86/TZ94p) levels and corrected the BDEs for ZPE but not for BSSE. These results are listed in Table 3. These MP2 calculations are comparable to the present MP2(TZ/DZ)BSSE calculations (MAD of 1.5 ± 1.4 kJ/mol, six values). Comparing the DFT calculations to our MP2(TZ/TZ)NoBSSE BDEs, we find that the BP86/TZ94p calculations are all lower than the current calculations, with a MAD of 17.0 ± 3.3 kJ/mol, while the SVWN/TZ94p calculations are in general higher than, but in better agreement with, the present calculations, with a MAD of 4.5 ± 3.8 kJ/mol. If we compare the DFT results to our MP2(TZ/DZ)BSSE calculations, the same trends are observed; however, the agreement is better for the BP86/TZ94p BDEs (MAD of 9.1 ± 5.3 kJ/mol) and worse for the SVWN/TZ94p BDEs (MAD of 12.2 ± 5.6 kJ/mol).

Feller et al.[70] conducted a theoretical study to estimate the MP2 complete basis set limit (CBS) for the BDEs of the $M^+(C_6H_6)$ complexes (M = Li through Cs) using a series of well-defined basis sets that are known to approach the CBS limit. This was accomplished using three diffuse-function-augmented correlation-consistent basis sets of double-, triple-, and quadruple-ζ quality (aug-cc-pVxZ, x = D, T, Q, respectively) with the use of the Hay−Wadt ECP for the Rb^+ and Cs^+ core electrons. The CBS limits, which were also corrected for core/valence and higher-order correlation [CCSD(T)] effects, are listed in Table 3. The CBS limits were derived from calculated binding energies that were not corrected for BSSE. A comparison to our MP2(TZ/DZ)BSSE and MP2(TZ/TZ)-NoBSSE calculations yields reasonable agreement, with MADs of 11.4 ± 4.7 and 5.6 ± 3.7 kJ/mol, respectively. The agreement between the CBS limits and our experimentally determined BDEs for $M^+(C_6H_6)$ is somewhat disappointing, with a MAD of 9.4 ± 5.3 kJ/mol (five values). There are no systematic trends: some calculated values are higher than experimental values, and some are lower. Surprisingly, the agreement between our calculated BDEs and the experimental BDEs is slightly better, with MADs of 9.0 ± 6.5 and 5.8 ± 2.6 kJ/mol for the MP2(TZ/DZ)BSSE (six values) and MP2(TZ/TZ)NoBSSE (six values) BDEs, respectively. It therefore seems apparent that even highly sophisticated CBS extrapolation methods cannot completely reproduce the experimental BDEs of the alkali-metal ion−mono-benzene complexes. This may be because of limitations in the degree of electron correlation and the need to rely on ECPs for the larger ions.

To our knowledge, Bauschlicher and Partridge (BP)[71] have reported the only previous theoretical study involving a bis-benzene complex of an alkali-metal ion, $Na^+(C_6H_6)_2$, performed using a small basis set (RHF/4-31G*//RHF/STO-3G) and no electron correlation. Also, it was not specified whether the calculated BDE was corrected for ZPE or BSSE. Surprisingly, and perhaps somewhat fortuitously, the $Na^+(C_6H_6)_2$ BDE calculated by BP (72.0 kJ/mol) is very close to our MP2(TZ/DZ)BSSE value, Table 3, and in reasonable agreement with the experimental BDE.

Comparison with Bond Dissociation Energies of Alkali-Metal−Water, Alkali-Metal−Dimethyl Ether (DME), and Transition Metal−Benzene Complexes. A comparison of the alkali-metal ion−benzene BDEs with previously determined experimental BDEs for $M^+(H_2O)_x$ and $M^+[O(CH_3)_2]_x$ complexes (M = Li through Cs, $x = 1-2$) is displayed in Figure 6. The BDEs for the $M^+[O(CH_3)_2]_x$ complexes[21,36−39] and $M^+(H_2O)_x$ complexes where M = Li[37,72] and Na[73] are taken from previous CID studies in our laboratory. The BDEs for the $M^+(H_2O)_x$ complexes where M = K through Cs are taken from HPMS studies of Kebarle and co-workers.[16,66]

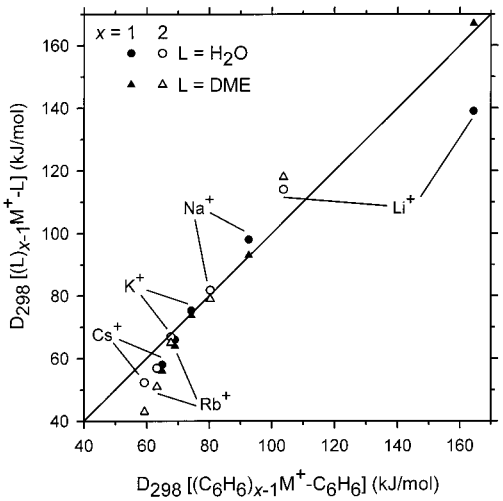

Figure 6. Experimental bond dissociation energies at 298 K of alkali-metal $(C_6H_6)_{x-1}M^+-C_6H_6$ vs $(L)_{x-1}M^+-L$ complexes, for $x = 1$ (closed symbols), $x = 2$ (open symbols), L = H_2O (circles), and L = $O(CH_3)_2$ (triangles). The bond dissociation energies for $(C_6H_6)_{x-1}M^+-C_6H_6$ are taken from Table 4, while the bond dissociation energies for $(L)_{x-1}M^+-L$ (L = H_2O and $O(CH_3)_2$) are taken from various references described in the text.

It can be seen from Figure 6 that the $M^+(H_2O)_x$ and $M^+[O(CH_3)_2]_x$ BDEs possess trends similar to those observed for the $M^+(C_6H_6)_x$ systems, i.e., a monotonic decrease in the BDE as the metal is changed from Li^+ to Cs^+. Furthermore, the decrease in sequential BDE is largest for Li^+ complexes. The BDEs of the $M^+(C_6H_6)_x$ complexes are observed to be comparable to or slightly lower than those of the $M^+(H_2O)_x$ and $M^+[O(CH_3)_2]_x$ complexes when M = Li through K, with the obvious exception of $Li^+(H_2O)$, but are larger when M = Rb and Cs. The former observation illustrates the strength of the ion−quadrupole and ion-induced dipole interactions in the $M^+(C_6H_6)_x$ complexes, comparable to the ion−dipole and ion-induced dipole interactions in the $M^+(H_2O)_x$ and $M^+[O(CH_3)_2]_x$ complexes. Just as the large difference in the BDE of $Li^+[O(CH_3)_2]$ relative to that of $Li^+(H_2O)$ was explained in terms of polarizability differences,[21] the stronger BDE for $Li^+(C_6H_6)$ compared to that for $Li^+(H_2O)$ is also believed to reflect the much larger polarizability of C_6H_6, 9.99 Å^3, relative to that of H_2O, 1.45 Å^3.[74] On the basis of the distance scaling of ion−dipole, ion−quadrupole, and ion-induced dipole interactions, r^{-2}, r^{-3}, and r^{-4}, respectively, and the inherently larger metal−ligand distances in the $M^+(C_6H_6)_x$, $M^+(H_2O)_x$, and $M^+[O(CH_3)_2]_x$ complexes with M = Rb and Cs, lower BDEs might have been expected for the Rb^+ and Cs^+ complexes with benzene compared to the BDEs for the complexes with polar water and dimethyl ether ligands. The observed trend can be rationalized by the larger diameter of the Rb^+ and Cs^+ metal ions,[60] which can overlap better with the diffuse π cloud of the benzene ring. This could enhance the bonding of these complexes relative to the bonding of water and dimethyl ether ligands (two-electron donors) by making C_6H_6 a more effective six-electron donor.

It is also instructive to compare the $M^+(C_6H_6)_x$ BDEs when M is an alkali metal to those when M is a transition metal. The sum of the sequential 0 K transition metal benzene BDEs, $D_0[M^+-C_6H_6] + D_0[(C_6H_6)M^+-C_6H_6]$, determined from a previous study in our laboratory,[52] were found to possess magnitudes between 511 ± 20 (M = Ti) and 336 ± 18 kJ/mol (M = Mn). In contrast to this, the sum of the sequential 0 K alkali-metal benzene BDEs (Table 3) is largest for the Li^+ complexes, 265 ± 15 kJ/mol, and decreases down the periodic column (123 ± 9 kJ/mol for the Cs^+ complexes). This clearly demonstrates the enhancement of the bond strengths from the donation of the transition metal 3d electrons into the π^* orbitals of benzene, i.e., metal−ligand back-bonding.

Conclusions

Bond dissociation energies of $M^+(C_6H_6)_x$ complexes (M = Li through Cs, $x = 1-2$) are determined by threshold collision-induced dissociation using a guided ion beam mass spectrometer after careful consideration of the effects of the reactant internal energy, the multiple collisions with Xe, and the lifetime of the ionic reactants (phase space limit transition state model). Both the absolute $M^+-C_6H_6$ and $(C_6H_6)M^+-C_6H_6$ bond dissociation energies and the change in sequential $M^+(C_6H_6)_x$ bond dissociation energies are observed to decrease monotonically upon changing the metal ion from Li^+ to Cs^+. These trends are explained in terms of the electrostatic nature of the bonding in the $M^+(C_6H_6)_x$ complexes and the changes in magnitude of the ligand−ligand interactions in the $M^+(C_6H_6)_2$ complexes, respectively. Theoretical values of the $M^+(C_6H_6)_x$ bond energies are also determined by ab initio calculations performed at the MP2(full)/6-311+G(2d,2p)//MP2(full)/6-31G* and MP2(full)/6-311+G(2d,2p)//MP2(full)/6-311+G* levels of theory for M = Li through K and with effective core potential/valence basis sets for K, Rb, and Cs. The agreement between experiment and theory is reasonably good for the all electron calculations, but significant, systematic deviations are observed with the use of the ECP basis sets for the metals. Similar observations hold for comparisons between the $M^+(C_6H_6)_x$ bond dissociation energies of the current work and the theoretical BDEs in literature. Our experimental $M^+(C_6H_6)_x$ BDEs agree well with previous literature values where data are available, except for the BDE of $Na^+(C_6H_6)$ reported previously by Castleman and coworkers.[14] Comparisons made to experimental BDEs of alkali-metal−water complexes, $M^+(H_2O)_x$, and alkali-metal−dimethyl ether complexes, $M^+[O(CH_3)_2]_x$, reveal comparable BDEs for $M^+(C_6H_6)_x$ when $M^+ = Li^+$, Na^+, and K^+ and larger BDEs when $M^+ = Rb^+$, Cs^+. The former observation is a result of comparable strengths of the electrostatic interactions in the $M^+(C_6H_6)_x$, $M^+(H_2O)_x$, and $M^+[O(CH_3)_2]_x$ complexes, whereas the latter observation indicates enhanced overlap of the larger ions with the aromatic π orbitals of benzene compared to those of the smaller metal ions.

Acknowledgment. Funding for this work was provided by the National Science Foundation under Grant CHE-9877162. The authors thank David Feller, David Dixon, and John Nicholas for providing a copy of their work prior to publication. An allocation of computer time from the Center for High Performance Computing at the University of Utah is gratefully acknowledged. The SGI Origin 2000 system at the Center for High Performance Computing is funded in part by the SGI Supercomputing Visualization Center Grant.

Supporting Information Available: Vibrational frequencies and average vibrational energies at 298 K of C_6H_6 and $M^+(C_6H_6)_x$ ($x = 1$ and 2), determined from vibrational analysis at the MP2(full)/6-31G* level; rotational constants for the energized complex and transition state for all $M^+(C_6H_6)_x$ complexes studied; figures for the six $M^+(C_6H_6)_x$ systems studied but not explicitly shown in the paper. This material is available free of charge via the Internet at http://pubs.acs.org.

References and Notes

(1) *Principles of Molecular Recognition*; Buckingham, A. D., Legon, A. C., Roberts, S. M., Eds.; Blackie Academic: Glasgow, 1993.
(2) *Comprehensive Supramolecular Chemistry*; Atwood, J. L., Davies, J. E. D., MacNicol, D. D., Vögtle, F., Lehn, J.-M., Eds.; Elsevier Science: Tarrytown, NY, 1996; Vol. 1 and 2.
(3) *Metal-Ion Separation and Preconcentration*; Bond, A. H., Dietz, M. L., Rodgers, R. D., Eds.; ACS Symposium Series 716; American Chemical Society: Washington, DC, 1999.
(4) Ma, J. C.; Dougherty, D. A. *Chem. Rev.* **1997**, *97*, 1307.
(5) Harrowfield, J. M.; Ogden, M. I.; Richmond, W. R.; White, A. H *J. Chem. Soc., Chem. Commun.* **1991**, 1159.
(6) Assmus, R.; Böhmer, V.; Harrowfield, J. M.; Ogden, M. I.; Richmond, W. R.; Skelton, B. W.; White, A. H *J. Chem. Soc., Dalton Trans.* **1993**, 2427.
(7) (a) Ikeda, A.; Shinkai, S. *J. Am. Chem. Soc.* **1994**, *116*, 3102. (b) Ikeda, A.; Tsuzuki, H; Shinkai, S. *Tetrahedron Lett.* **1994**, *35*, 8417. (c) Inokuchi, F; Miyahara, Y.; Inazu, T.; Shinkai, S. *Angew. Chem., Int. Ed. Engl.* **1995**, *34*, 1364.
(8) Lhoták, P.; Shinkai, S. *J. Phys. Org. Chem.* **1997**, *10*, 273.
(9) (a) Shepodd, T. J.; Petti, M. A.; Dougherty, D. A. *J. Am. Chem. Soc.* **1986**, *108*, 6085. (b) Shepodd, T. J.; Petti, M. A.; Dougherty, D. A. *J. Am. Chem. Soc.* **1988**, *110*, 1983. (c) Petti, M. A.; Shepodd, T. J.; Berrans, R. E., Jr.; Dougherty, D. A. *J. Am. Chem. Soc.* **1988**, *110*, 6825. (d) Kearny, P. C.; Mizoe, L. S.; Kumpf, R. A.; Forman, J. E.; McCurdy, A.; Dougherty, D. A. *J. Am. Chem. Soc.* **1993**, *115*, 9907.
(10) Dougherty, D. A. *Science* **1996**, *271*, 163.
(11) Scrutton, N. S.; Raine, A. R. C. *Biochem. J.* **1996**, *319*, 1.
(12) Woodin, R. L.; Beauchamp, J. L. *J. Am. Chem. Soc.* **1978**, *100*, 501.
(13) Taft, R. W; Anvia, F.; Gal, J.-F.; Walsh, S.; Capon, M.; Holmes, M. C.; Hosn, K.; Oloumi, G.; Vasanwala, R.; Yazdani, S. *Pure Appl. Chem.* **1990**, *62*, 17.
(14) Guo, B. C.; Purnell, J. W.; Castleman, A. W., Jr. *Chem. Phys. Lett.* **1990**, *168*, 155.
(15) Armentrout, P. B.; Rodgers, M. T. *J. Phys. Chem. A* **2000**, *104*, 2238.
(16) Sunner, J; Nishizawa, K; Kebarle, P. *J. Phys. Chem.* **1981**, *85*, 1814.
(17) Ervin, K. M.; Armentrout, P. B. *J. Chem. Phys.* **1985**, *83*, 166.
(18) Schultz, R. H.; Armentrout, P. B. *Int. J. Mass Spectrom. Ion Processes* **1991**, *107*, 29.
(19) Muntean, F.; Armentrout, P. B. Unpublished results.
(20) Teloy, E.; Gerlich, D. *Chem. Phys.* **1974**, *4*, 417. Gerlich, D. Diplomarbeit, University of Freiburg, Freiburg, Germany, 1971.
(21) More, M. B.; Glendening, E. D.; Ray, D.; Feller, D.; Armentrout, P. B. *J. Phys. Chem.* **1996**, *100*, 1605.
(22) Ray, D.; Feller, D.; More, M. B.; Glendening, E. D.; Armentrout, P. B. *J. Phys. Chem.* **1996**, *100*, 16116.
(23) Loh, S. K.; Lian, L.; Hales, D. A.; Armentrout, P. B. *J. Chem. Phys.* **1988**, *89*, 3378.
(24) Schultz, R. H.; Crellin, K. C.; Armentrout, P. B. *J. Am. Chem. Soc.* **1991**, *113*, 8590.
(25) Dalleska, N. F.; Honma, K.; Sunderlin, L. S.; Armentrout, P. B. *J. Am. Chem. Soc.* **1994**, *116*, 3519.
(26) Dalleska, N. F.; Honma, K.; Armentrout, P. B. *J. Am. Chem. Soc.* **1993**, *115*, 12125.
(27) Khan, F. A.; Clemmer, D. C.; Schultz, R. H.; Armentrout, P. B. *J. Phys. Chem.* **1993**, *97*, 7978.
(28) (a) Schultz, R. H.; Armentrout, P. B. *J. Chem. Phys.* **1992**, *96*, 1046. (b) Fisher, E. R.; Kickel, B. L.; Armentrout, P. B. *J. Phys. Chem.* **1993**, *97*, 10204.
(29) (a) Beyer, T. S.; Swinehart, D. F. *Comm. Assoc. Comput. Machines* **1973**, *16*, 379. (b) Stein, S. E.; Rabinovitch, B. S. *J. Chem. Phys.* **1973**, *58*, 2438. (c) Stein, S. E.; Rabinovitch, B. S. *Chem. Phys. Lett.* **1977**, *49*, 1883.
(30) (a) Pople, J. A.; Schlegel, H. B.; Raghavachari, K.; DeFrees, D. J.; Binkley, J. F.; Frisch, M. J.; Whitesides, R. F.; Hout, R. F.; Hehre, W. J. *Int. J. Quantum Chem. Symp.* **1981**, *15*, 269. (b) DeFrees, D. J.; McLean, A. D. *J. Chem. Phys.* **1985**, *82*, 333.
(31) Rodgers, M. T.; Armentrout, P. B. *J. Phys. Chem. A* **1997**, *101*, 2614.
(32) Rodgers, M. T.; Ervin, K. M.; Armentrout, P. B. *J. Chem. Phys.* **1997**, *106*, 4499.
(33) Waage, E. V.; Rabinovitch, *Chem. Rev.* **1970**, *70*, 377.

(34) Chesnavich, W. J.; Bowers, M. T. *J. Phys. Chem.* **1979**, *83*, 900.
(35) Armentrout, P. B. In *Advances in Gas-Phase Ion Chemistry*; Adams, N. G., Babcock, L. M., Eds.; JAI: Greenwich, U.K., 1992; Vol. 1, pp 83−119 and references therein.
(36) More, M. B.; Ray, D.; Armentrout, P. B. *J. Phys. Chem A.* **1997**, *101*, 831.
(37) Rodgers, M. T.; Armentrout, P. B. *J. Phys. Chem A.* **1997**, *101*, 1238.
(38) More, M. B.; Ray, D.; Armentrout, P. B. *J. Phys. Chem A.* **1997**, *101*, 4254.
(39) More, M. B.; Ray, D.; Armentrout, P. B. *J. Phys. Chem A.* **1997**, *101*, 7007.
(40) For example, see Figure 1 in ref 26.
(41) Armentrout, P. B.; Simons, J. *J. Am. Chem. Soc.* **1992**, *114*, 8627.
(42) Frisch, M. J.; Trucks, G. W.; Schlegel, H. B.; Scuseria, G. E.; Robb, M. A.; Cheeseman, J. R.; Zakrzewski, V. G.; Montgomery, J. A., Jr.; Stratmann, R. E.; Burant, J. C.; Dapprich, S.; Millam, J. M.; Daniels, A. D.; Kudin, K. N.; Strain, M. C.; Farkas, O.; Tomasi, J.; Barone, V.; Cossi, M.; Cammi, R.; Mennucci, B.; Pomelli, C.; Adamo, C.; Clifford, S.; Ochterski, J.; Petersson, G. A.; Ayala, P. Y.; Cui, Q.; Morokuma, K.; Malick, D. K.; Rabuck, A. D.; Raghavachari, K.; Foresman, J. B.; Cioslowski, J.; Ortiz, J. V.; Stefanov, B. B.; Liu, G.; Liashenko, A.; Piskorz, P.; Komaromi, I.; Gomperts, R.; Martin, R. L.; Fox, D. J.; Keith, T.; Al-Laham, M. A.; Peng, C. Y.; Nanayakkara, A.; Gonzalez, C.; Challacombe, M.; Gill, P. M. W.; Johnson, B. G.; Chen, W.; Wong, M. W.; Andres, J. L.; Head-Gordon, M.; Replogle, E. S.; Pople, J. A. *Gaussian 98*, Revision A.7; Gaussian, Inc.: Pittsburgh, PA, 1998.
(43) The Hay−Wadt valence basis sets and effective core potentials were obtained from the Extensible Computational Chemistry Environment Basis Set Database (www.emsl.pnl.gov:2080/forms/basisform.html), as developed and distributed by the Molecular Science Computing Facility, Environmental and Molecular Sciences Laboratory, which is part of the Pacific Northwest National Laboratory, P.O. Box 999, Richland, WA 99352, and funded by the U.S. Department of Energy. For the original valence basis set and ECP reference, see: Hay, P. J.; Wadt, W. R. *J. Chem. Phys.* **1985**, *82*, 299.
(44) Glendening, E. D.; Feller, D.; Thompson, M. A. *J. Am. Chem. Soc.* **1994**, *116*, 10657.
(45) Hoyau, S.; Norman, K.; McMahon, T. B.; Ohanessian, G. J. *J. Am. Chem. Soc.* **1999**, *121*, 8864.
(46) Walter, D.; Armentrout, P. B. *J. Am. Chem. Soc.* **1998**, *120*, 3176.
(47) Gilbert, R. G.; Smith, S. C. *Theory of Unimolecular and Recombination Reactions*; Blackwell Scientific Publications: Oxford, 1990.
(48) Foresman, J. B.; Frisch, Æ. *Exploring Chemistry with Electronic Structure Methods*, 2nd ed.; Gaussian Inc.: Pittsburgh, PA, 1996.
(49) (a) Boys, S. F.; Bernardi, R. *Mol. Phys.* **1970**, *19*, 553. (b) Van Duijneveldt, F. B.; van Duijneveldt-van de Rijdt, J. G. C. M.; van Lenthe, J. H. *Chem. Rev.* **1994**, *94*, 1873.
(50) In the case of $K^+(C_6H_6)$, there were products formed that had masses consistent with fragmentation of the benzene ring, but these only appeared at energies higher than 4.6 eV and possessed cross magnitudes less than 0.25 $Å^2$.
(51) For results of a $M^+(CO)_x$ + Ar (M = Li, Na, K) CID study in which the M^+−Ar thresholds were analyzed and found to be lower than the M^+−CO thresholds by the values of the M^+−Ar bond dissociation energies, see: Walter, D.; Sievers, M. R.; Armentrout, P. B. *Int. J. Mass Spectrom. Ion Processes* **1998**, *175*, 93.
(52) Meyer, F.; Khan, F. A.; Armentrout, P. B. *J. Am. Chem. Soc.* **1995**, *117*, 9740.
(53) (a) Schultz, R. H.; Armentrout, P. B. *J. Phys. Chem.* **1993**, *97*, 596. (b) Haynes, C. L.; Armentrout, P. B.; Perry, J. K.; Goddard, W. A., III. *J. Phys. Chem.* **1995**, *99*, 6340. (c) Khan, F. A.; Steele, D. L.; Armentrout, P. B. *J. Phys. Chem.* **1995**, *99*, 7819. (d) Meyer, F.; Chen, Y.-M.; Armentrout, P. B. *J. Am. Chem. Soc.* **1995**, *117*, 4071. (e) Sievers, M.; Armentrout, P. B. *J. Phys. Chem.* **1995**, *99*, 8135. (f) Goebel, S.; Haynes, C. L.; Khan, F. A.; Armentrout, P. B. *J. Am. Chem. Soc.* **1995**, *117*, 6994.
(54) Lifshitz, C. *Adv. Mass Spectrom.* **1989**, *11*, 113.
(55) Rodgers, M. T.; Armentrout, P. B. *Int. J. Mass Spectrom. Ion Processes* **1999**, *185*/*186*/*187*, 359.
(56) (a) Rodgers, M. T.; Armentrout, P. B. *J. Phys. Chem. A* **1999**, *103*, 4955. (b) Andersen, A.; Muntean, F.; Walter, D.; Rue, C.; Armentrout, P. B. *J. Phys. Chem. A* **2000**, *104*, 692.
(57) For example, the reanalysis of the Li^+(*t*-ButOH) + Xe primary CID cross section (which exhibited a kinetic shift of 0.29 eV; see ref 31) with the perpendicular internal rotational parameters treated as a single 2-D rotor resulted in a threshold value which was decreased by 0.03 eV compared to the value when these parameters are treated as two 1-D rotors.
(58) Benson, S. W. *Thermochemical Kinetics*; Wiley: New York, 1976; p 49.
(59) The metal ring−centroid distance is defined as the distance from the metal atom to the central point within the benzene ring that is in the plane of the carbon atoms.
(60) Wilson, R. G.; Brewer, G. R. *Ion Beams: With Applications to Ion Implantation*; Wiley: New York, 1973; pp 118−124.
(61) Rodgers, M. T.; Armentrout, P. B. *J. Am. Chem. Soc.* **2000**, *122*, 8548.
(62) Feller, D.; Glendening, E. D.; Woon, D. E.; Feyereisen, M. W. *J. Chem. Phys.* **1995**, *103*, 3526.
(63) Feller, D.; Aprà, E.; Nichols, J. A.; Bernholdt, D. E. *J. Phys. Chem.* **1996**, *105*, 1940.
(64) Feller, D. *Chem. Phys. Lett.* **2000**, *322*, 543.
(65) These temperature corrections were calculated in the same manner as the correction factors listed in Table 4 for conversion from 0 to 298 K.
(66) Dzidic, I.; Kebarle, P. *J. Phys. Chem.* **1970**, *74*, 1466.
(67) Rodgers, M. T.; Armentrout, P. B. *J. Chem. Phys.* **1998**, *109*, 1787.
(68) Castleman, A. W., Jr. Personal communication.
(69) Nicholas, J. B.; Hay, B. P.; Dixon, D. A. *J. Phys. Chem. A* **1999**, *103*, 1394.
(70) Feller, D.; Dixon, D. A.; Nicholas, J. B. *J. Phys. Chem. A* **2000**, *104*, 11414.
(71) Bauschlicher, C. W., Jr.; Partridge, H. *J. Phys. Chem.* **1991**, *95*, 9694.
(72) Rodgers, M. T.; Armentrout, P. B. *J. Chem. Phys.* **1998**, *109*, 1787.
(73) Dalleska, N. F.; Tjelta, B. L.; Armentrout, P. B. *J. Phys. Chem.* **1994**, *98*, 4193.
(74) Rothe, E. W.; Berstein, R. B. *J. Chem. Phys.* **1959**, *31*, 1619.